ARTICLE IN PRESS

Engineering Structures ▮ (▮▮▮▮) ▮▮▮–▮▮▮

Contents lists available at ScienceDirect

Engineering Structures

journal homepage: www.elsevier.com/locate/engstruct

Shear strength of R/C bridge cantilever slabs

R. Vaz Rodrigues [a,*], M. Fernández Ruiz [b], A. Muttoni [b]

[a] Fellrath & bosso sa ingénieurs civils, ch. de maillefer 37 - cp 190 ch - 1050 le mont-sur-lausanne, Switzerland

[b] Ecole Polytechnique Fédérale de Lausanne, IS–BETON, bât. GC, Station 18, CH-1015, Lausanne, Switzerland

ARTICLE INFO

Article history:
Received 27 January 2008
Received in revised form
11 April 2008
Accepted 14 April 2008
Available online xxxx

Keywords:
Shear strength
Tests
Cantilevers
Concentrated loads
Shear field
Reinforced concrete slabs

ABSTRACT

This paper presents the results of six tests on R/C bridge cantilever slabs without shear reinforcement subjected to concentrated loading. The specimens represent actual deck slabs of box-girder bridges scaled 3/4. They were 10 m long with a clear cantilever equal to 2.78 m and with variable thickness (190 mm at the tip of the cantilever and 380 mm at the clamped edge). Reinforcement ratios for the specimens were equal to 0.78% and 0.60%. All tests failed in a brittle manner by development of a shear failure surface around the concentrated loads. The experimental results are investigated on the basis of linear elastic shear fields for the various tests. Taking advantage of the experimental and numerical results, practical recommendations for estimating the shear strength of R/C bridge cantilever slabs are proposed.

1. Introduction

Reinforced concrete slabs without shear reinforcement are commonly used in many structural systems, such as bridge deck slabs (Fig. 1(a), (b)), flat slabs of buildings, parking garages (Fig. 1(c), (d)) and cut-and-cover tunnels. Shear is usually the governing failure mode at ultimate of R/C slabs without transverse reinforcement [1]. One-way shear is found for distributed loading and close to support lines, where parallel shear forces in the slab develop (Fig. 1(b)). On the contrary, two-way shear (also known as punching shear) is associated to concentrated loading, since shear forces develop radially to introduce the load in the slab (Fig. 1(c)). Intermediate cases between one- and two-way shear, where shear forces in a slab develop neither parallel nor radially [2–4] are also found in practice. This is the case for instance of cantilever deck slabs of bridges subjected to concentrated loading or of edge columns of flat slabs, where the development of shear forces depends on boundary and loading conditions (Fig. 1(a), (d)).

Currently, codes of practice provide several approaches to check the one- and the two-way shear strength of flat slabs. Such approaches (see Appendix for ACI 318-05 [5] and EC2 2004 [6]) typically propose a similar format, where the design shear strength (V_R) is estimated by multiplying a shear strength per unit length (nominal shear strength, v_R) by a control perimeter (b_0):

$$V_R = v_R \cdot b_0. \quad (1)$$

However, the strength of intermediate cases between one- and two-way shear is not always covered by current codes of practice. This is for instance the case of cantilever deck slabs of bridges subjected to concentrated loading (Fig. 1(a)) where the control perimeter to be introduced into Eq. (1) is usually not defined. Also, scanty experimental data is available for such members. Lu [7] performed a series of tests on relatively small cantilevers with constant thickness of 50 and 60 mm. Vaz Rodrigues [8] tested (prior to the tests presented in this paper) a half-scale specimen representing the cantilever deck slab of a bridge. The specimen had variable thickness (110–140 mm), a clear span of 1.0 m and it was subjected to concentrated loading. Failure in this test was due to the development of a shear failure surface around the concentrated load.

In this paper, the results of six 3/4-scale tests on R/C cantilever slabs subjected to concentrated loading are presented with the aim of providing experimental data on this topic. The specimens had a significant size (see Fig. 2) with a thickness similar to that of actual cantilever deck slabs of bridges (thickness of the specimens varying between 190 mm at the tip and 380 mm at the clamped edge, refer to Fig. 3). This allowed to correctly account for the size effect in shear (decreasing nominal shear strength with increasing size of the member) and thus to investigate whether failure developed in shear or bending. Based on test results and on the elastic shear field estimated for the various tests, a suitable control perimeter is defined to check the shear strength of cantilever slabs using the format proposed in Eq. (1). This perimeter can be adopted in combination with ACI 318-05 [5] and EC2 2004 [6] punching shear formulations for practical design purposes.

* Corresponding author. Tel.: +41 79 211 38 81.
E-mail addresses: rui.vazrodrigues@fbsa.ch, rui.vazrodrigues@gmail.com (R. Vaz Rodrigues), miguel.fernandezruiz@epfl.ch (M. Fernández Ruiz), aurelio.muttoni@epfl.ch (A. Muttoni).

0141-0296/$ – see front matter © 2008 Elsevier Ltd. All rights reserved.
doi:10.1016/j.engstruct.2008.04.017

Notation

The following symbols are used in this paper:

E_c	modulus of elasticity of concrete
Q	applied load
Q_R	applied load at failure
$Q_{R,\text{test}}$	measured load at failure
V	shear force
V_R	shear force at failure
$V_{R,\text{test}}$	measured shear force at failure on the governing control perimeter
V_{ACI}	shear strength according to ACI 318-05 [5] formulation of the nominal shear strength
$V_{ACI,\text{elast}}$	shear strength according to ACI 318-05 [5] formulation of the nominal shear strength for a control perimeter based on the elastic shear field
$V_{ACI,3-S}$	shear strength according to ACI 318-05 [5] formulation of the nominal shear strength for a three-sided control perimeter
V_{EC2}	shear strength according to EC2 2004 [6] formulation of the nominal shear strength
$V_{EC2,\text{elast}}$	shear strength according to EC2 2004 [6] formulation of the nominal shear strength for a control perimeter based on the elastic shear field
$V_{EC2,3-S}$	shear strength according to EC2 2004 [6] formulation of the nominal shear strength for a three-sided control perimeter
b_0	length of control perimeter
$b_{0,\text{elast}}$	length of control perimeter based on linear-elastic shear fields
$b_{0,3-S}$	length of a three-sided control perimeter
d	effective depth (distance from extreme compression fibre to the centroid of the longitudinal tensile reinforcement)
d_b	nominal diameter of bar
f_c	compressive strength of concrete measured on cylinders
f_{ct}	tensile strength of concrete
f_u	tensile strength of reinforcement
f_y	yield strength of reinforcement
h	thickness of the slab
v_0	magnitude of the principal shear force
v_{el}	magnitude of the linear-elastic shear force acting perpendicular to the control perimeter
$v_{el,\max}$	maximum value of v_{el} along the control perimeter
v_R	shear strength per unit length of control perimeter (nominal shear strength)
v_x	shear force per unit length (xz surface)
v_y	shear force per unit length (yz surface)
w	deflection of the slab
x, y	coordinate axes
ξ	factor accounting for size effect (EC2 2004 [6])
ε_u	reinforcement strain at rupture
φ_0	direction of the principal shear force
ρ	flexural reinforcement ratio

2. Test campaign

2.1. Test specimens

Tests were performed on two R/C slabs with variable thickness and without shear reinforcement. The specimens represent actual deck slabs of box-girder bridges scaled 3/4. Each slab was tested three times varying the position and the number of applied concentrated loads, see Table 1 and Fig. 3.

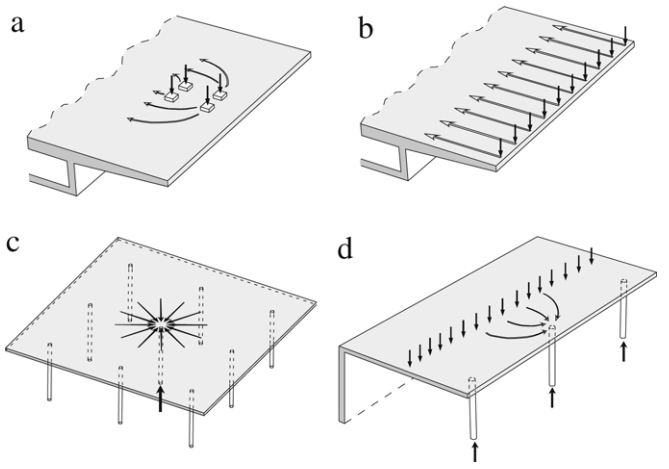

Fig. 1. One- and two-way shear in slabs: (a) cantilever bridge deck slab subjected to concentrated loading; (b) cantilever bridge deck slab subjected to line loading; (c) flat slab supported by columns; and (d) flat slab supported by columns and a wall.

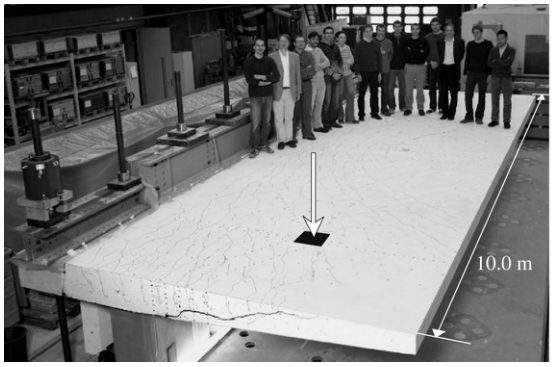

Fig. 2. View of specimen DR2 after testing.

For cantilever DR1, the transverse top reinforcement at the clamped edge consisted of 16 mm diameter bars spaced 75 mm (reinforcement ratio $\rho = 0.78\%$). For cantilever DR2, the transverse top reinforcement at the same position consisted of 14 mm diameter bars spaced 75 mm (reinforcement ratio $\rho = 0.60\%$). Only one half of the transverse top reinforcement continued to the free edge of the cantilever. The other half was cut-off at 1380 mm from the clamped edge for both cantilevers, see Fig. 3. The bottom reinforcement in both directions and the longitudinal top reinforcement consisted of 12 mm diameter bars spaced 150 mm for the two slabs. The bottom bars in the transverse direction were bent up at the free edge and anchored in the top layer. The clear concrete cover was 30 mm.

2.2. Material properties

Normal strength concrete was used in both slabs. The compressive strength, modulus of elasticity and tensile strength of concrete are detailed in Table 2 together with the age of concrete at the time of testing. The properties of concrete were measured on concrete cylinders (320 mm high, 160 mm diameter). The compressive strength of concrete at the time of testing ranged from 38.9 to 42.4 MPa and the average modulus of elasticity was 36.6 GPa (secant stiffness between compressive stresses 1 to 10 MPa). The tensile strength (average value equal to 3.0 MPa) was obtained from direct tension tests. The composition of one cubic

Table 1
Performed tests: Number of concentrated loads, reinforcement ratios and failure loads

Slab	Test	Number of concentrated loads	Transverse reinforcement ratio for top bars at clamped edge	Sum of concentrated loads at failure $Q_{R,test}$ (kN)
DR1	DR1-a	4	0.78%	1397
	DR1-b	2		1025
	DR1-c	1		910
DR2	DR2-a	2	0.60%	961
	DR2-b	2		857
	DR2-c	1		719

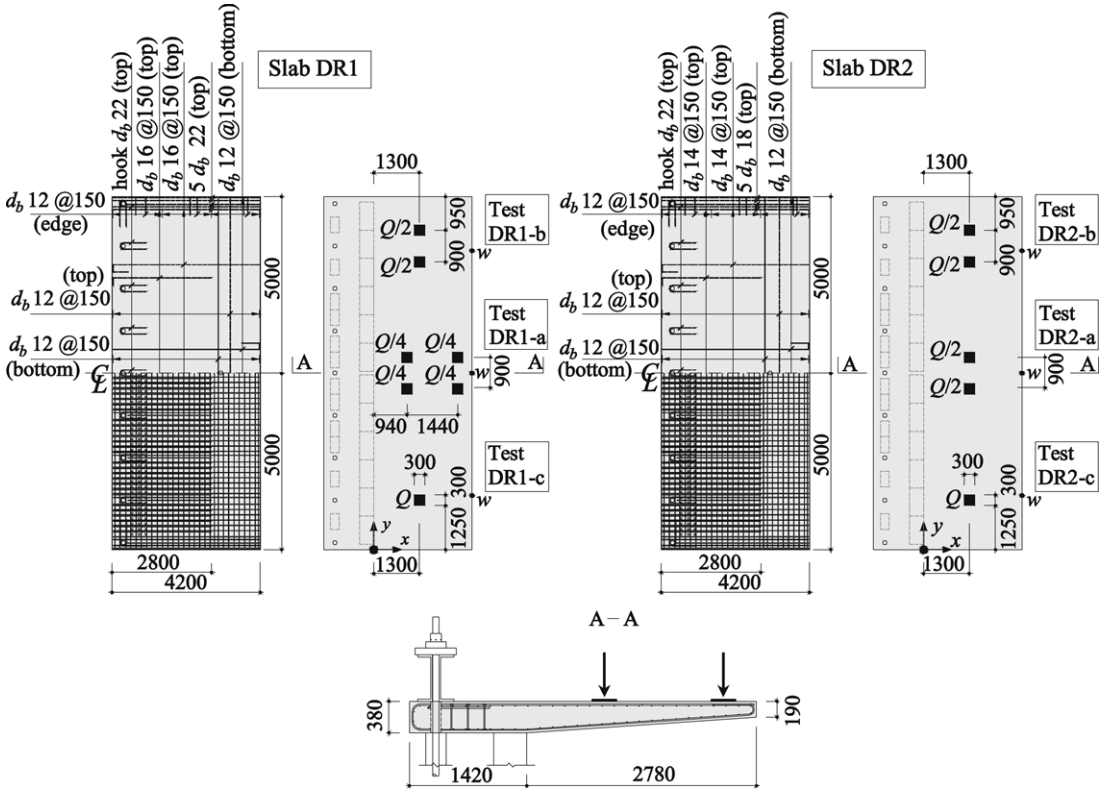

Fig. 3. Geometry, reinforcement layout and applied loads for both specimens (dimensions in [mm], axis *x*: transverse direction; axis *y*: longitudinal direction).

Table 2
Measured properties of concrete

Test	Age at testing (days)	f_c (MPa)	f_{ct} (MPa)	E_c (GPa)
DR1-a	76	39.1	2.9	36.0
DR1-b	92	39.9	3.0	36.1
DR1-c	114	40.8	3.1	36.2
DR2-a	66	38.9	3.1	36.3
DR2-b	105	42.0	3.1	37.4
DR2-c	112	42.4	3.1	37.5

meter of concrete was 753 kg of sand, 604 kg of gravel ranging from 4 to 8 mm diameter, 661 kg of gravel ranging from 8 to 16 mm diameter, 325 kg of portland cement and 174 kg of water. The maximum size of the aggregate was 16 mm.

The mechanical properties of the reinforcement measured for various bar diameters are detailed in Table 3. All bars were hot-rolled (well-defined yield plateau) except for 12 mm bars of slab DR2 that were cold-worked.

2.3. Test set-up

Fig. 4 shows the test set-up for test DR1-a, with four concentrated forces (scaled also 3/4 with respect to the load configuration according to Eurocode 1, 2003 [9]). The distance between the loads in the transverse direction was 1440 mm and 900 mm in the longitudinal direction (it should be noted that the distance 1440 mm – imposed by the length of the available beams in the laboratory – is slightly smaller than 1500 mm, which is the exact 3/4 scale). The load was introduced by a hollow hydraulic jack connected to a hand pump. The jack was anchored to the laboratory strong floor by a 75 mm diameter bar, where spherical nuts and washers were used to accommodate rotation. The load was transmitted to the slab through steel plates (300 × 300 × 30 mm) using one beam in the transverse direction and two spreaders in the longitudinal direction. For the tests with two concentrated forces (DR1-b, DR2-a and DR2-b), the load introduction system was similar but the spreaders were removed and the steel beam was rotated 90° (with the beam thus placed directly above the load cells). For the tests with one concentrated force (DR1-c and DR2-c), the steel beam was also removed and the load was applied directly to a steel plate.

2.4. Measurements

Continuous measurements of the applied forces were taken both at the steel plates where the load was introduced and at the hydraulic jack. This allowed for redundancy in force measurements and to determine the actual load applied at each plate [10]. Also, other continuous measurements were taken (see Fig. 5 for test DR2-a): deflections of the slab with linearly variable

Table 3
Measured properties of reinforcing steel

Slab	d_b (mm)	f_y (MPa)	f_u (MPa)	ε_u[a] (%)	f_u/f_y	Reinforcement type
DR1	16	499	600	10.7	1.20	Hot-rolled
	12	541	629	9.05	1.16	Hot-rolled
	22	534	644	10.9	1.21	Hot-rolled
DR2	14	505	591	11.1	1.17	Hot-rolled
	12	469[b]	580	5.19	1.24	Cold-worked
	18	541	639	11.5	1.18	Hot-rolled

[a] Measurement length 150 mm.
[b] Offset yield stress at 0.2% strain.

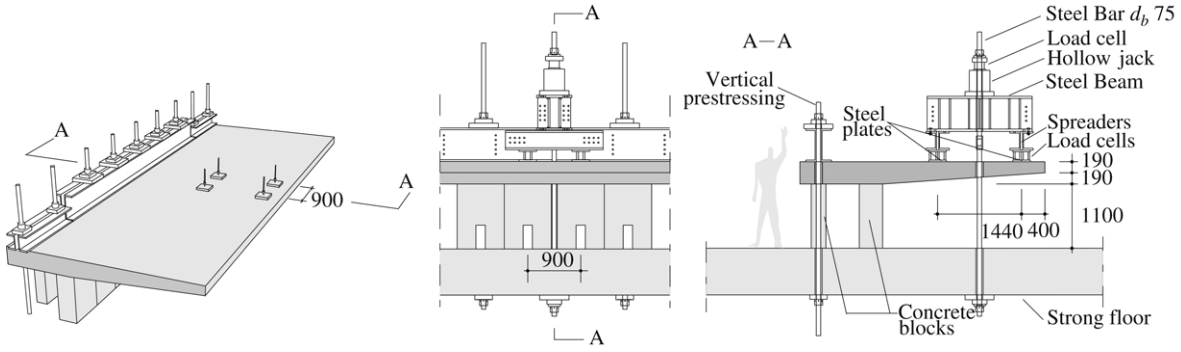

Fig. 4. Test set-up for test DR1-a, dimensions in [mm].

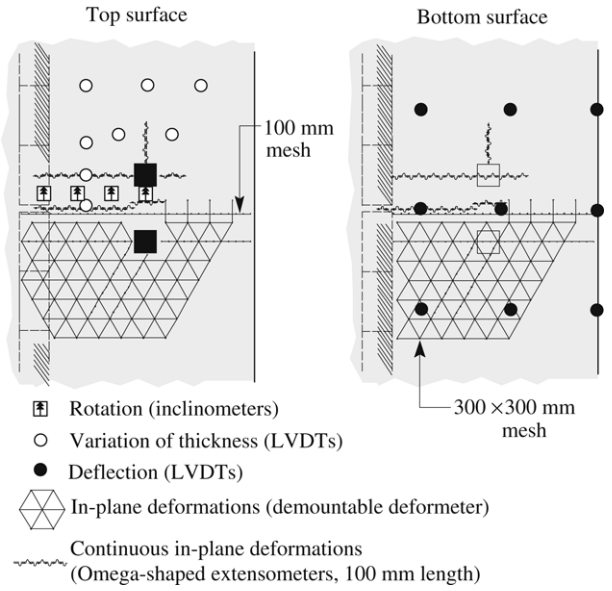

Fig. 5. Measurements of deflections, rotations, variation of thickness and in-plane deformations (test DR2-a).

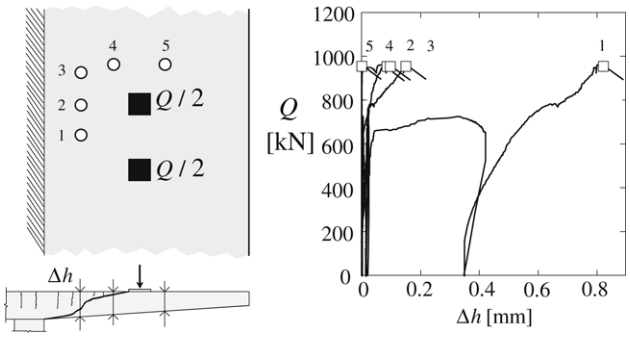

Fig. 6. Measured increase of the thickness of the slab for test DR2-a.

displacement transducers (LVDTs); rotation measurements with inclinometers; variation of the thickness of the slab with LVDTs and measurements of the strains at the upper and lower surfaces of the slab with omega-shaped gauges (glued to the concrete surface, base length equal to 100 mm).

In-plane displacement readings were taken at selected load stages between aluminium targets of a triangular mesh both in the top and in the bottom surfaces of the slab (base length equal to 300 mm, see Fig. 5). These displacements were measured using portable LVDT devices (digital demec strain gauges). Also, displacement readings were taken at the same load stages along lines in the transverse direction (base length equal to 100 mm), see Fig. 5.

After testing, the slabs were saw-cut allowing to observe the shape of the failure surface in the cross section of the slab. Thereafter, the specimens were separated along the failure surface, which was three-dimensionally mapped (for all slabs except DR1-a) using a laser device and a measuring grid with about six hundred positions.

2.5. Test development

First flexural cracks developed for all tests on the top surface at the clamped edge (cracks along the longitudinal direction). Such cracks increased their widths during the test, reaching at failure values between 0.3 mm (test DR1-c) and 1.8 mm (test DR1-a). At the bottom surface, cracks developed below the applied loads following the transverse direction. The maximal crack openings measured on the bottom surface prior to failure ranged between 0.2 mm (tests DR2-b and DR-2a) and 1.0 mm (DR1-a). Taking into account the values of the measured crack widths, significant yielding occurred in the top and in the bottom reinforcement for test DR1-a [11]. On the contrary, none or very limited yielding occurred for the other tests, with crack openings at failure smaller than 0.6 mm.

The increase in the thickness of the slab was also recorded, see test DR2-a in Fig. 6. At about 50% of the failure load, the

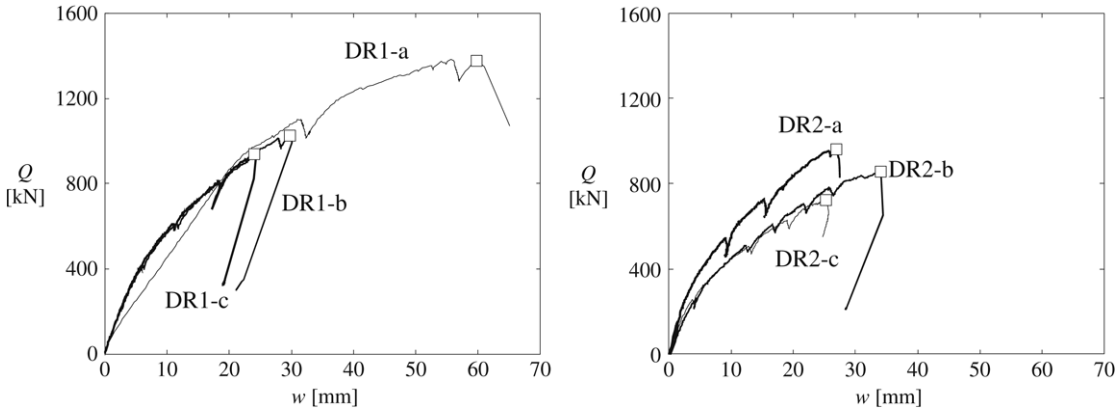

Fig. 7. Load–deflection curves for all tests.

thickness of the slab started to increase, reaching at failure (961 kN) a maximum value of about 0.8 mm.

The load–deflection curves for all tests are shown in Fig. 7, where the deflection w is given at the free edge of the cantilever (Fig. 3). It can be noted that a plastic plateau was not attained for any of the tests (and thus the yield-line pattern was not fully developed for any of the tests). More details on the test measurements can be found in [10].

2.6. Failure mode

All tests failed by development of a shear failure surface around the concentrated loads in a brittle manner. The failure load ($Q_{R,\text{test}}$, sum of the applied concentrated forces at failure) are given in Table 1. It can be noted that, for tests performed with the same number of forces and boundary conditions, shear strength decreases with decreasing flexural reinforcement ratios.

Fig. 8 shows the geometry of shear failure surfaces, including the position of shear cracks in the cross-section. For test DR1-a, the failure surface developed around the two concentrated loads near the tip of the cantilever, see Figs. 8 and 9. For this test, another shear crack developed in the region between the clamped edge and the concentrated loads (Fig. 8). This latter crack, however, did not develop a complete failure surface. Fig. 9(a)–(c) show the crack pattern for test DR1-a seen from top prior to failure (Fig. 9(c)) and from bottom after cutting of the specimen (Fig. 9(b)). For tests DR1-b-c and DR2-b-c, the shear crack was clearly visible after failure at the free edges, see Fig. 9(d). No significant interference between the inclined shear failure surfaces of the various tests was noticed after cutting of the specimens, see Fig. 8.

3. Analysis of the test results

3.1. Shear field in flat slabs

The shear field is a vector field representing the direction (ϕ_0) and magnitude (v_0) of the principal shear force per unit length in a slab [12,13]. With respect to reinforced concrete slabs, a sandwich model [14] is particularly useful to explain the physical meaning of parameters v_0 and ϕ_0. A sandwich model (Fig. 10(a)) considers a slab divided into three regions: a core carrying shear forces (Fig. 10(b)) and two outer panels (Fig. 10(c)) carrying compression and tension forces (thus equilibrating internal bending and torsion moments).

With respect to the core, shear forces per unit length acting in the cross-section (v_x and v_y) are in equilibrium with in-plane shear forces developed in upper and lower faces of the core, see Fig. 10(b). Such in-plane shear forces are in turn in equilibrium with force-increments acting in the panels as shown in Fig. 10(c). The in-plane shear forces (v_x and v_y) are two vectors whose resultant is the principal shear force, defined by its magnitude (v_0) and by its in-plane direction (φ_0). Such values can thus be calculated as (Fig. 10(d)):

$$\varphi_0 = \arctan\left(\frac{v_y}{v_x}\right) \tag{2}$$

$$v_0 = \sqrt{v_x^2 + v_y^2}. \tag{3}$$

It can be noted that the in-plane principal shear force is in equilibrium with the cross-section principal shear force in the core of the sandwich, which has the same magnitude (v_0) and develops in a plane perpendicular to the direction φ_0 (Fig. 10(c)).

The shear field can be represented by a set of lines parallel at each point with the shear field direction (φ_0) and whose thickness is proportional to its magnitude (v_0), see [11]. Such a plot helps in understanding the shear forces developing in a slab. For instance, Fig. 11 shows the shear fields for three of the tests presented in this paper (DR1-a, DR2-b and DR2-c) assuming a linear-elastic behaviour of the slab (uncracked concrete). In this figure, the direction of the principal shear forces developing along a control perimeter at $d/2$ from the edge of the load plates is also plotted (by a set of arrows) together with the magnitude of the shear force acting perpendicular to the perimeter (v_{el}) and its maximum value ($v_{el,\max}$). It should be noted that the integral of v_{el} along the control perimeter (shear flow) equals the total applied load inside the control perimeter. Analyses presented in Fig. 11 are performed using the finite element program ANSYS® Academic Research product [15] with element type Shell 43 and they are post-processed using MatLab® [16] to plot the shear fields.

It can be noted that the distribution of shear forces along the control perimeters is clearly uneven, and is influenced by boundary conditions (position of the clamped and of the free edges with respect to the applied loads). Potential zones where punching shear failure may develop can be investigated on the basis of the shear fields. For instance, comparing the actual failure planes of the slabs (Fig. 8) to the elastic shear fields (Fig. 11), it can be noted that shear failure surfaces developed in regions with the largest magnitude of shear force.

3.2. Control perimeter on the basis of shear fields

To account for non-uniform distribution of shear forces developing in the control perimeter (Fig. 11), Vaz Rodrigues [11]

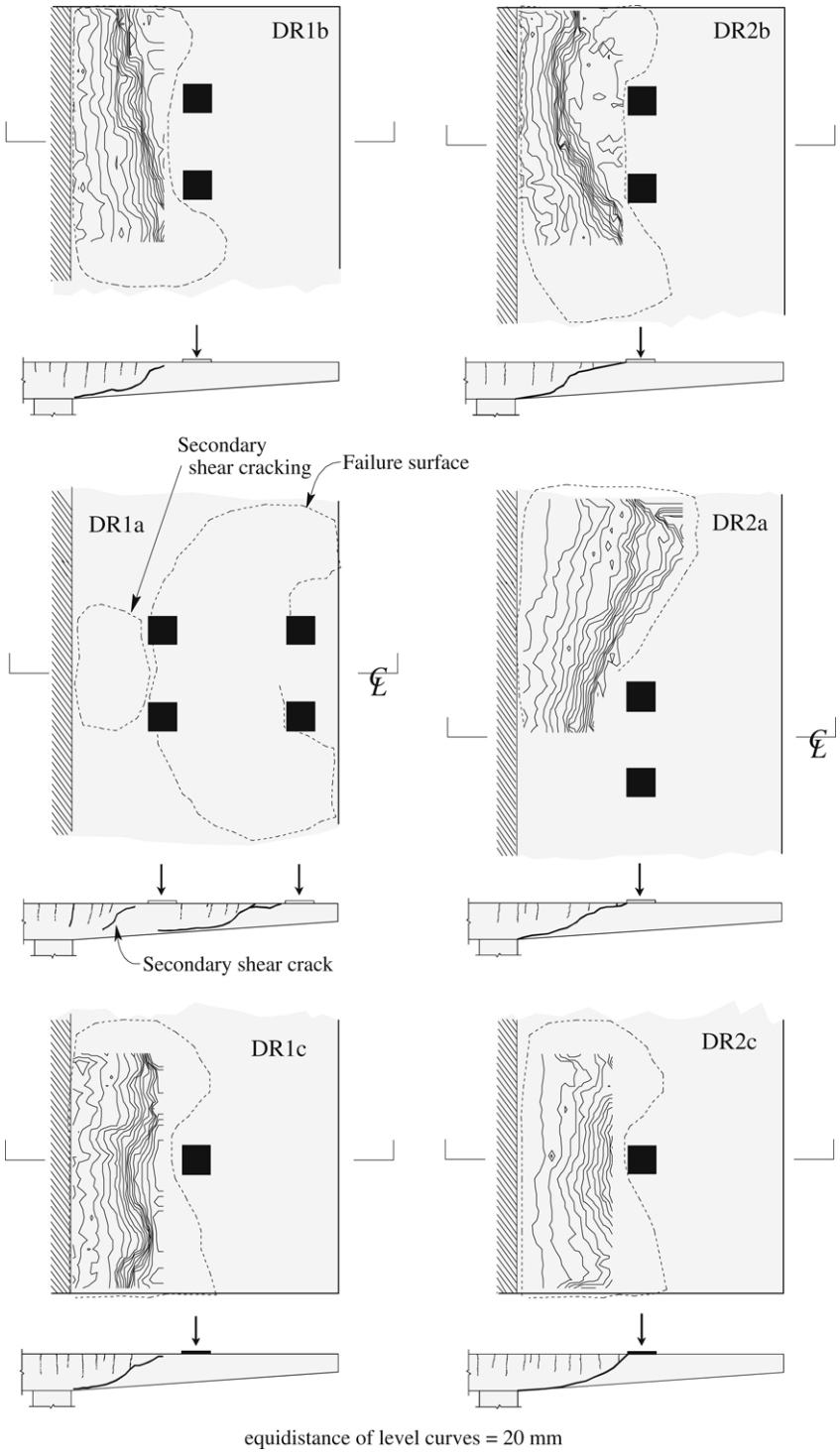

Fig. 8. Failure surfaces after cutting of the slabs.

proposes to reduce the control perimeter according to the following expression:

$$b_{0,\text{elast}} = \frac{V}{v_{el,\max}}. \quad (4)$$

This approach is in fact equivalent to considering that the shear force per unit length is constant along the reduced control perimeter, being its value equal to $v_{el,\max}$. It can be noted that, for a linear-elastic analysis and if self-weight is neglected, this perimeter is constant since $v_{el,\max}$ depends linearly on V.

Redistributions in the shear field [17] due to concrete cracking or due to yielding of the reinforcement are not considered according to Eq. (4). This approach leads thus to a conservative estimate of the shear strength of a member [11].

Table 4 summarizes the values of $b_{0,\text{elast}}$ obtained using Eq. (4) for the various tests presented in this paper for control perimeters at $d/2$ and $2d$ from the border of the loading plates. For practical purposes, it can be noted that a reasonable estimate of the length of the control perimeters derived from Eq. (4) ($b_{0,\text{elast}}$) is obtained assuming simple three-sided control perimeters ($b_{0,3-s}$, see Fig. 12

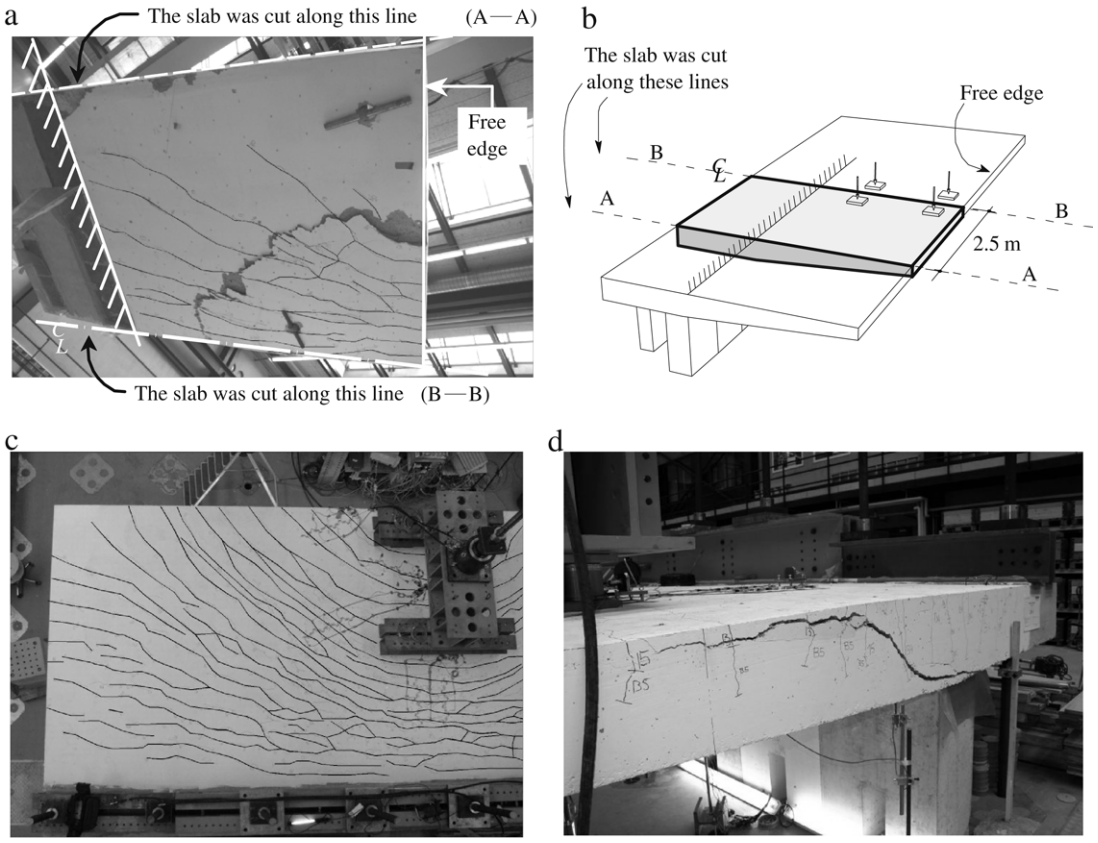

Fig. 9. Crack pattern and shear cracks: (a) view from bottom of slab DR1 (test DR1-a) after cutting the slab; (b) view of saw-cut of slab DR1-a; (c) crack pattern prior to failure in the top surface of test DR1-a; and (d) side view of the shear crack after failure of test DR1-b.

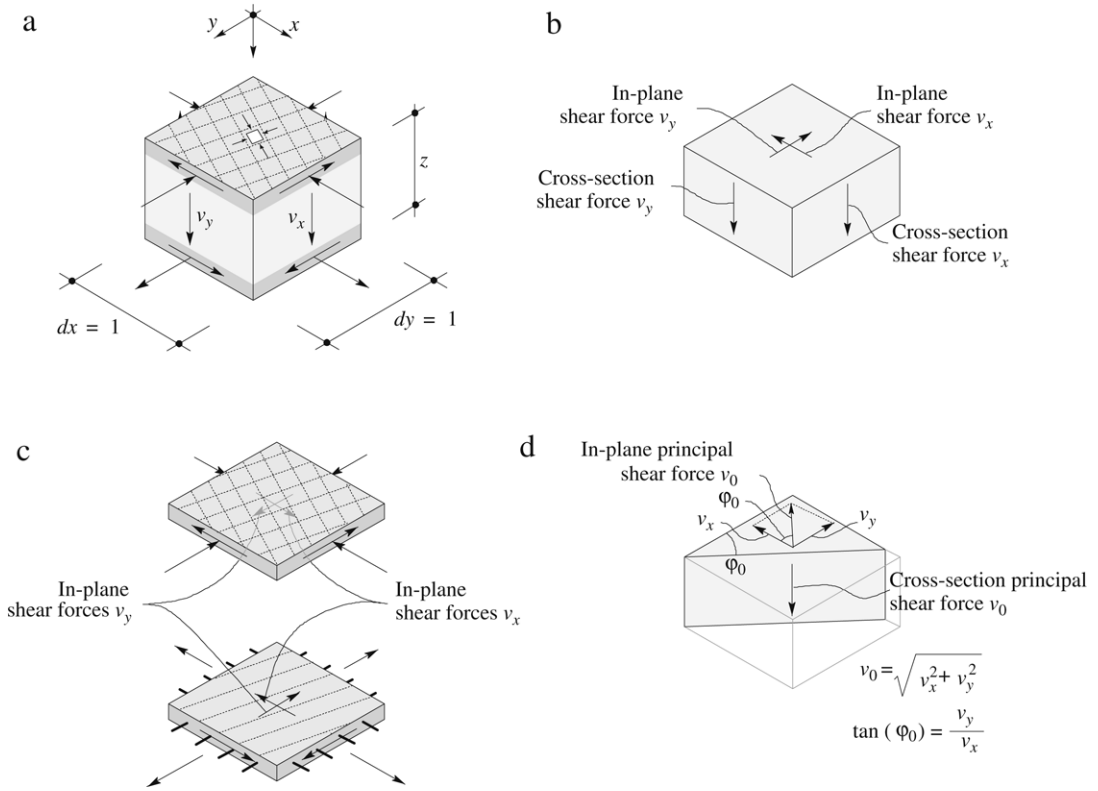

Fig. 10. Sandwich model of a reinforced concrete slab element: (a) general view of the element; (b) forces acting on the core; (c) forces acting on the panels; and (d) magnitude and direction of the principal shear force.

Please cite this article in press as: Vaz Rodrigues R, et al. Shear strength of R/C bridge cantilever slabs. Engineering Structures (2008), doi:10.1016/j.engstruct.2008.04.017

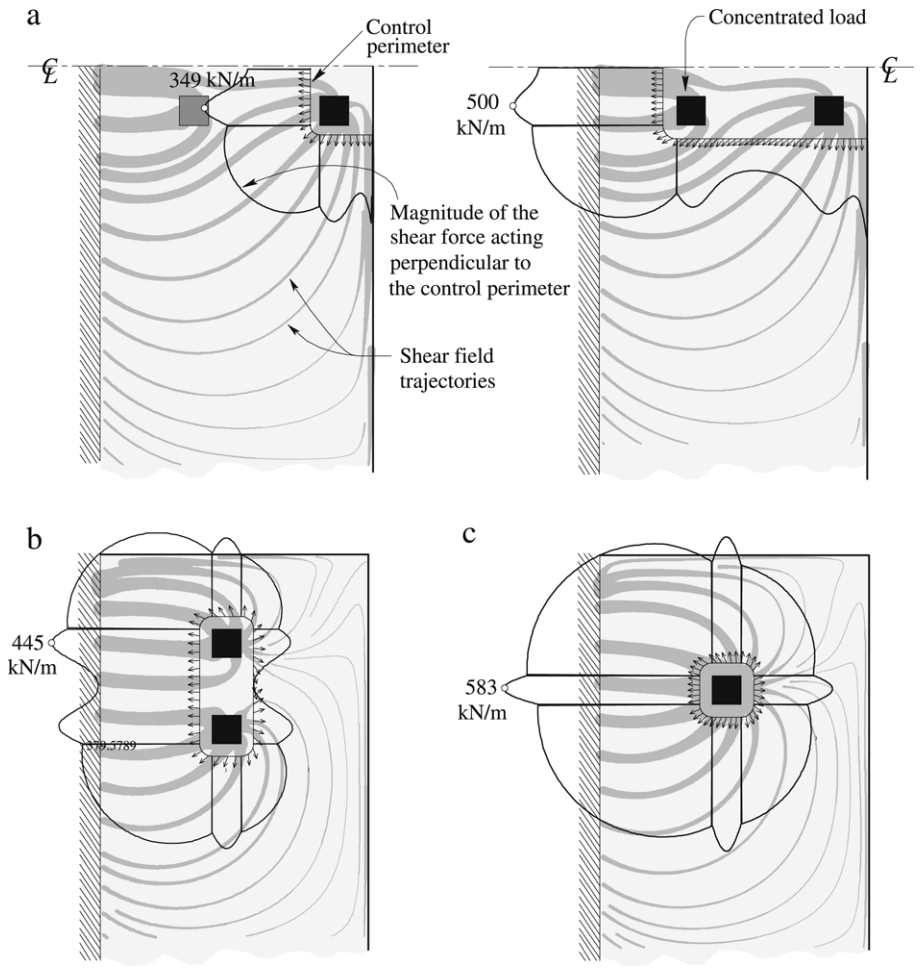

Fig. 11. Linear elastic distribution of shear forces (kN/m, including self-weight) along control perimeters at $d/2$ of the applied loads: (a) test DR1-a ($Q = 1397$ kN); (b) test DR2-b ($Q = 857$ kN); and (c) test DR2-c ($Q = 719$ kN).

Table 4
Control perimeters based on linear-elastic shear fields (see Fig. 11 and Eq. (4)) and comparison to three-sided control perimeters at $d/2$ and $2d$ of the border of the applied loads (see Fig. 12)

Test	d (m)	Control perimeter at $d/2$			Control perimeter at $2d$		
		$b_{0,\text{elast}}$ (m)	$b_{0,3-S}$ (m)	$b_{0,\text{elast}}/b_{0,3-S}$	$b_{0,\text{elast}}$ (m)	$b_{0,3-S}$ (m)	$b_{0,\text{elast}}/b_{0,3-S}$
DR1-a[a]	0.171	2.00	1.55	1.29	3.02	2.35	1.29
DR1-a[b]	0.221	2.79	2.71	1.03	3.03	3.75	0.81
DR1-b	0.245	1.94	1.96	0.99	2.52	2.84	0.89
DR1-c	0.245	1.24	1.28	0.97	2.05	2.43	0.84
DR2-a	0.247	2.14	1.97	1.09	2.90	3.13	0.93
DR2-b	0.247	1.94	1.97	0.98	2.51	3.13	0.80
DR2-c	0.247	1.24	1.29	0.96	2.05	2.45	0.84
			Avge	1.04			0.91
			CoV	0.11			0.19

[a] Control perimeter around two concentrated loads near the tip of the cantilever.
[b] Control perimeter around four concentrated loads.

and Table 4). For both cases, a similar average value of the ratio $b_{0,\text{elast}}/b_{0,3-S}$ is obtained with a larger (yet reasonable) scatter of the results for the perimeter at $2d$.

3.3. Comparison to design codes

The strength according to Eq. (1) using the punching shear strength formulations of ACI 318-05 (control perimeter at $d/2$ from the border of the loading plates) and EC2 2004 (control perimeter at $2d$ from the border of the loading plates) are summarized in Table 5. The results are given for both control perimeters obtained from Eq. (4) (based on the elastic shear-fields) and for three-sided control perimeters, where the values of the effective depth in Table 5 are taken at the centre of gravity of the applied loads. For EC2 2004, the flexural reinforcement ratio corresponds to the top transverse reinforcement since this reinforcement governs the width of the critical shear crack developing through the failure surface as shown in Fig. 8.

It should be noted that for beams or slabs subjected to one-way shear, the inclination of the compression chord can carry a non-negligible fraction of the shear forces [18]. However, this effect is neglected in this case as shear forces are developing all around the control perimeter (Fig. 11).

Please cite this article in press as: Vaz Rodrigues R, et al. Shear strength of R/C bridge cantilever slabs. Engineering Structures (2008), doi:10.1016/j.engstruct.2008.04.017

Table 5
Comparison between actual and computed shear strengths

Test	$V_{R,\text{test}}$ (kN)	d (m)	ρ (%)	Control perimeter at $d/2$				Control perimeter at $2d$			
				$V_{ACI,\text{elast}}$ (kN)	$V_{R,\text{test}}/V_{ACI,\text{elast}}$	$V_{ACI,3-S}$ (kN)	$V_{R,\text{test}}/V_{ACI,3-S}$	$V_{EC2,\text{elast}}$ (kN)	$V_{R,\text{test}}/V_{EC2,\text{elast}}$	$V_{EC2,3-S}$ (kN)	$V_{R,\text{test}}/V_{EC2,3-S}$
DR1-a[a]	698	0.171	0.78	714	0.98	553	1.26	582	1.20	453	1.54
DR1-b	1025	0.245	1.09	1000	1.02	1011	1.01	745	1.38	839	1.22
DR1-c	910	0.245	1.09	647	1.41	668	1.36	610	1.49	723	1.26
DR2-a	961	0.247	0.83	1099	0.87	1012	0.95	780	1.23	842	1.14
DR2-b	857	0.247	0.83	1035	0.83	1051	0.81	693	1.24	864	0.99
DR2-c	719	0.247	0.83	665	1.08	692	1.04	567	1.27	678	1.06
			Avge		1.03		1.07		1.30		1.20
			CoV		0.20		0.19		0.09		0.16

[a] Control perimeter around two concentrated loads near the tip of the cantilever.

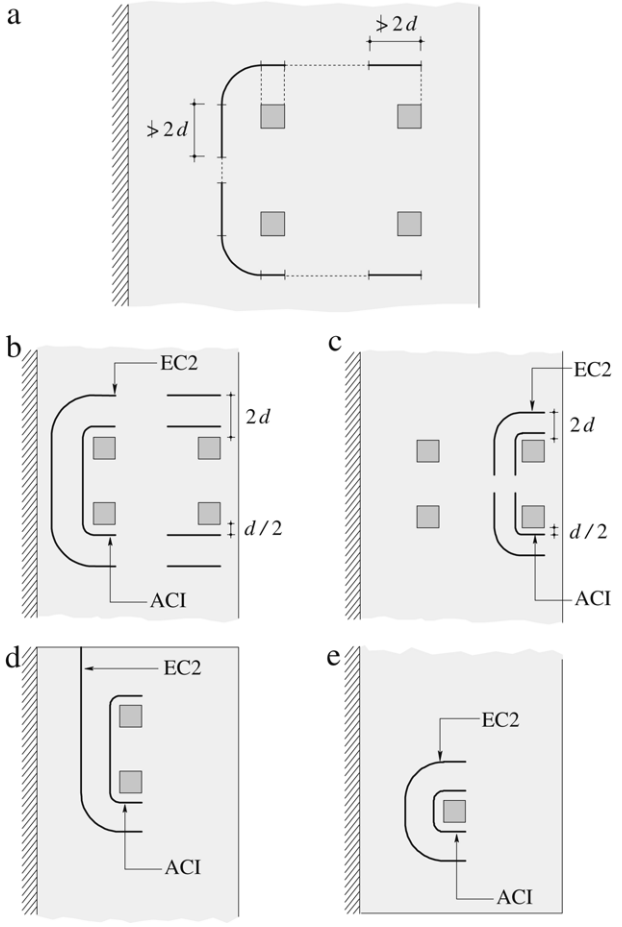

Fig. 12. Three-sided control perimeters used with ACI-318-05 [5] and EC2 2004 [6]: (a) generic perimeter; (b) perimeter for test DR1-a considering the four concentrated loads; (c) perimeter for test DR1-a around the concentrated loads near the tip of the cantilever and for test DR2-a; (d) perimeter for tests DR1-b and DR2-b; and (e) perimeter for tests DR1-c and DR2-c.

Good agreement with conservative results is obtained using control perimeters based on elastic shear fields and three-sided control perimeters together with both EC2 2004 and ACI 318-05 formulations of the nominal shear strength (v_R). For test DR1a, the critical perimeter is the one around the two loads applied at the tip of the cantilever as shown in Fig. 12(c). For this test, the strength for the perimeter with four loads inside (Fig. 12(b)) is not governing due to the increase on the length of the control perimeter and on the effective depth. In addition, a larger flexural reinforcement ratio (which increases the shear strength according to EC2 2004, see Appendix) is to be considered for the perimeter with four loads inside than for to the perimeter with two loads inside.

It is interesting to note that ACI 318-05 provides somewhat conservative estimates for tests with larger reinforcement ratios (tests DR1a-c) whereas less conservative estimates are obtained for smaller reinforcement ratios (tests DR2a-c). This is due to the fact that ACI punching shear formulation does not consider the influence of the reinforcement ratio in the punching shear strength. On the other hand this influence is included in EC2 leading to a smaller scatter of the results. Also, it should be noted that ACI 318-05 does not consider the influence of size effect in its formulation (see Appendix). Consequently, and although good results are obtained for the tests presented in this paper, unsafe estimates of shear strength for slabs with larger thicknesses can be obtained using ACI 318-05 [1]. With respect to EC2, rather conservative estimates are obtained using control perimeters based on elastic shear fields. This can be explained by the fact that the control perimeter is placed at a certain distance of the border of the loading plates ($2d$), where significant shear field redistributions [17] can develop. Further research on this topic is still open.

Comparisons to the test results presented in this paper and to other test results using the control perimeter given by Eq. (4) together with the shear and punching shear formulations proposed by the critical shear crack theory [1] can also be found in [10].

3.4. Application to practical cases

With respect to the actual application of the proposed approach to check the shear strength of cantilever deck slabs of bridges, the influence of other phenomena should also be taken into account:

- The presence of edge beams, which modify the shear field especially in the region close to the tip of the cantilever. Its influence as a function of their stiffness with respect to the cantilever slab is investigated in [11]. An experimental study on the influence of edge beams on the strength of cantilever deck slabs subjected to concentrated loading can be found in [8].
- The effect of longitudinal bending of the bridge, which develops compression forces (near mid-span) or tension forces (near the support region) along the longitudinal direction of the cantilever slab. This effect should be taken into account when checking the shear strength as it increases (slab in compression) or reduces (slab in tension) the nominal shear strength [19]. Both ACI 318-05 and EC2 2004 formulations allow considering this influence.

4. Conclusions

This paper investigates the strength and behaviour of R/C bridge cantilever slabs without transverse reinforcement subjected to concentrated loading. The results of six 3/4-scale tests are presented and discussed. The main conclusions of this paper are:

1. All tests failed in a brittle manner by development of a shear failure surface around concentrated loads.
2. As confirmed by crack width measurements, failure in shear developed in most specimens without yielding of the flexural reinforcement. Failure was thus attained before development of a flexural mechanism.
3. Test results confirm that shear strength increases with increasing reinforcement ratios.
4. The shear field is a useful tool to get an intuitive insight of the shear forces developing in a slab. On that basis, the failure region in slabs subjected to concentrated loads can be investigated.
5. A simple approach based on the shear field is proposed to estimate the control perimeter for punching shear in R/C slabs.
6. For practical purposes, a three-sided perimeter can be adopted for cantilever deck slabs subjected to concentrated loading. This approach leads to good and conservative results used in combination with punching shear formulations proposed by codes of practice ACI 318-05 [5] and EC2 2004 [6].

Acknowledgements

The authors would like to gratefully acknowledge the support and funding of the Swiss Federal Road Authority and the Fundação para a Ciência e a Tecnologia (Portugal), grant FCT/BD/13259/2003, which made the experimental and theoretical studies possible.

Appendix. Punching shear formulations of ACI 318-05 and EC2 2004

According to ACI 318-05 [5], the punching shear strength accounting for the dimensions of the reaction area can be estimated using:

$$V_R = \frac{1}{3} \cdot \sqrt{f_c} \cdot d \cdot b_0 \quad \text{(SI-Units: mm and N)} \tag{5}$$

where d is the effective depth of the member and f_c is the compressive strength of concrete (measured in cylinders).

According to EC2 2004 [6], the following formula can be adopted:

$$V_R = 0.18 \cdot d \cdot \xi \cdot (100 \cdot \rho_l \cdot f_c)^{1/3} \cdot b_0 \quad \text{(SI-Units: mm and N)} \tag{6}$$

where ρ_l is the flexural reinforcement ratio and ξ is a factor accounting for the size effect (decreasing nominal shear strength with increasing size of the member) defined by the following expression:

$$\xi = 1 + \sqrt{\frac{200\,[\text{mm}]}{d}} \leqslant 2.0. \tag{7}$$

References

[1] Muttoni A. Punching shear strength of reinforced concrete slabs without transverse reinforcement. ACI Struct J 2008; Farmington Hills, Mich. (in press).
[2] Oliveira DR, Regan PE, Melo GS. Punching resistance of RC slabs with rectangular columns. Mag Concrete Res 2004;40(3):123–38.
[3] Regan PE, Rezai-Jorabi H. Shear resistance of one-way slabs under concentrated loads. ACI Struct J 1988;85(2):150–7. Farmington Hills, Mich.
[4] Sherwood EG, Lubell AS, Bentz EC, Collins MP. One-way shear strength of thick slabs and wide beams. ACI Struct J 2006;103(6):794–802. Farmington Hills, Mich.
[5] ACI Commitee 318-05. Building code requirements for structural concrete. Farmington Hills, Mich: ACI American Concrete Institute; 2005.
[6] Eurocode 2. Design of concrete structures — Part 1-1: General rules and rules for buildings. Brussels, Belgium: CEN; 2004. EN 1992-1-1.
[7] Lu H-Y. Behaviour of reinforced concrete cantilevers under concentrated loads. Ph.D. thesis. University of Cambridge, Girton College, Cambridge, UK; 2003.
[8] Vaz Rodrigues R. Test of a reinforced concrete cantilever under a concentrated load (in French, Essai d'un porte-à-faux de pont sous charge concentrée, this report can be downloaded from http://is-beton.epfl.ch/publications). IS-BETON, Ecole Polytechnique Fédérale de Lausanne, Lausanne, Switzerland; 2002.
[9] Eurocode 1. Actions on structures — Part 2: Traffic loads on bridges. Brussels, Belgium: CEN; 2003. EN 1991-2.
[10] Vaz Rodrigues R, Muttoni A. Large scale tests on reinforced concrete bridge deck slabs, test report. IS-BETON, Ecole Polytechnique Fédérale de Lausanne, Lausanne, Switzerland; 2006.
[11] Vaz Rodrigues R. Shear strength of reinforced concrete bridge deck slabs. Ph.D. thesis. Nr 3739, IS-BETON, Ecole Polytechnique Fédérale de Lausanne, Lausanne, Switzerland; 2007.
[12] Marti P. Design of Concrete Slabs for Transverse Shear. ACI Structural Journal 1990;40(2):180–90. Farmington Hills, Mich.
[13] Marti P. Flow of forces in reinforced concrete slabs (in German: Kraftfluss in Stahlbetonplatten). Beton- und Stalbetonbau 2003;98(2):85–93.
[14] Muttoni A, Schwartz J, Thürlimann B. Design of concrete structures with stress fields. Switzerland: Birkhaüser; 1997.
[15] ANSYS® Academic research. release 10.0. Help system. ANSYS, Inc.
[16] MATLAB® Release 7.1. Help system. The MathWorks, Inc.
[17] Muttoni A, Fernández Ruiz M. Shear flow in R/C slabs (in German: Schubkraftfluss in Stahlbetonflachdecken). Bau und Wissen, Wildegg, Fachveranstaltung 864571/72, Bemessungsprobleme bei Flachdecken, Wildegg, Switzerland; 2007, 3.1-3.16.
[18] Fernández Ruiz M, Muttoni A. Shear strength of thin-webbed post-tensioned beams. ACI Struct J 2008;105(3):308–17. Farmington Hills, Mich.
[19] Regan PE. Punching shear in prestressed concrete slab bridges. Engineering Structures Research Group, Polytechnic of Central London; 1983.